Progress in Neurobiology 240 (2024) 102655

Contents lists available at ScienceDirect

Progress in Neurobiology

journal homepage: www.elsevier.com/locate/pneurobio

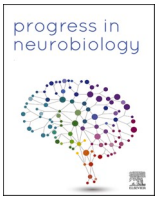

Population coding for figure-ground texture segregation in macaque V1 and V4

Xing-Nan Zhao [a,b,1], Xing-Si Dong [a,b,1], Dan-Qing Jiang [a,b], Si Wu [a,b,c], Shi-Ming Tang [b,c,d,*], Cong Yu [a,c,**]

[a] School of Psychological and Cognitive Sciences, Peking University, Beijing, China
[b] PKU-Tsinghua Center for Life Sciences, Peking University, Beijing, China
[c] IDG-McGovern Institute for Brain Research, Peking University, Beijing, China
[d] School of Life Sciences, Peking University, Beijing, China

ARTICLE INFO

Keywords:
Figure-ground perception
Texture segregation
V1/V4
Macaque
Two-photon imaging

ABSTRACT

Object recognition often involves the brain segregating objects from their surroundings. Neurophysiological studies of figure-ground texture segregation have yielded inconsistent results, particularly on whether V1 neurons can perform figure-ground texture segregation or just detect texture borders. To address this issue from a population perspective, we utilized two-photon calcium imaging to simultaneously record the responses of large samples of V1 and V4 neurons to figure-ground texture stimuli in awake, fixating macaques. The average response changes indicate that V1 neurons mainly detect texture borders, while V4 neurons are involved in figure-ground segregation. However, population analysis (SVM decoding of PCA-transformed neuronal responses) reveal that V1 neurons not only detect figure-ground borders, but also contribute to figure-ground texture segregation, although requiring substantially more principal components than V4 neurons to reach a 75 % decoding accuracy. Individually, V1/V4 neurons showing larger (negative/positive) figure-ground response differences contribute more to figure-ground segregation. But for V1 neurons, the contribution becomes significant only when many principal components are considered. We conclude that V1 neurons participate in figure-ground segregation primarily by defining the figure borders, and the poorly structured figure-ground information V1 neurons carry could be further utilized by V4 neurons to accomplish figure-ground segregation.

1. Introduction

Figure-ground segregation is crucial for object recognition because a potential object (figure) often needs to be distinguished from the surrounding stimuli before being recognized. When a figure lacks differentiation from the ground in first-order statistics, such as luminance and color, the brain can still perform figure-ground segregation effortlessly on the basis of second-order stimulus statistics such as texture (Julesz, 1981).

Previous research has suggested that V1 neurons are involved in segregating figure-ground stimuli formed by orientation-defined textures, as their responses to the figure are heightened compared to those to the ground (Lamme, 1995). This finding is supported by later single-unit studies (Zipser et al., 1996; Marcus and Van Essen, 2002) and fMRI studies (Poltoratski et al., 2019). However, Rossi, Desimone, and Ungerleider (Rossi et al., 2001) questioned this conclusion, noting that V1 responses were increased only when the size of the figure matched the size of the classical receptive fields of V1 neurons (~1°) when macaques were either fixating or performing a texture segregation task. They interpreted this as an indication of orientation discontinuity or border detection effects due to surround modulation, rather than figure-ground segregation, by V1 neurons.

Evidence for the involvement of V4 neurons in figure-ground texture segregation is more consistent. Electrode recordings have shown significant figure enhancement during figure-ground segregation in V4 neurons even without attention directed towards the figure (Poort et al., 2012, 2016). In addition, monkeys with V4 lesions have difficulty discriminating shapes composed of oriented lines (Merigan, 1996).

* Corresponding author at: School of Life Sciences, Peking University, Beijing, China.
** Corresponding author at: School of Psychological and Cognitive Sciences, Peking University, Beijing, China.
E-mail addresses: tangshm@pku.edu.cn (S.-M. Tang), yucong@pku.edu.cn (C. Yu).
[1] Equal-contribution first authors.

https://doi.org/10.1016/j.pneurobio.2024.102655
Received 1 January 2024; Received in revised form 9 June 2024; Accepted 30 June 2024
Available online 4 July 2024

In the current study, we re-explored the roles of V1 and V4 neurons in texture segregation from a population perspective. We recorded large samples of neurons in awake macaques using two-photon calcium imaging, which allowed for not only descriptive summaries with less sampling bias and higher statistical power than previous electrode recording data, but also machine learning analysis of population coding by V1 and V4 neurons. Using PCA-transformed data, we trained linear SVMs (support vector machines) to examine population coding of the texture border and the figure-ground by V1 and V4 neurons. We further studied the correlation between decoding weights and response characteristics of individual neurons. Our results show that, although V1 neurons are primarily involved in texture border detection, they also contribute to figure-ground segregation by carrying poorly structured figure-ground information, which may be readout by downstream V4 neurons to complete figure-ground segregation. These results help reconcile prior inconsistencies and shed light on the collaborative roles of V1 and V4 neurons in achieving figure-ground texture segregation.

2. Materials and methods

2.1. Monkey preparation

Monkey preparation was identical to procedures reported in our previous studies (Guan et al., 2021; Ju et al., 2021). Six rhesus monkeys (*Macaca mulatta*) aged 4–7 years underwent two sequential surgeries under general anesthesia and strictly sterile conditions. During the first surgery, a 20-mm diameter craniotomy was performed on the skull over V1 or dorsal V4. The craniotomy over V4 targeted the area encompassing the lunate sulcus (lu) and the terminal portion of the inferior occipital sulcus (io) (Fig. 1B). The dura was opened and multiple tracks of 100–150 nL AAV1.hSynap.GCaMP5G.WPRE.SV40 (AV-1-PV2478, titer 2.37e13 (GC/ml), Penn Vector Core) were pressure-injected at a depth of ~350 μm at multiple locations. To ensure uniform expression of GCaMP, the injection sites were spaced approximately 1 mm apart. The dura was then sutured, the skull cap was re-attached with three titanium lugs and six screws, and the scalp was sutured. After the surgery, the animal was returned to the cage and treated with injectable antibiotics (Ceftriaxone sodium, Youcare Pharmaceutical Group, China) for one week. Postoperative analgesia was also administered. The second

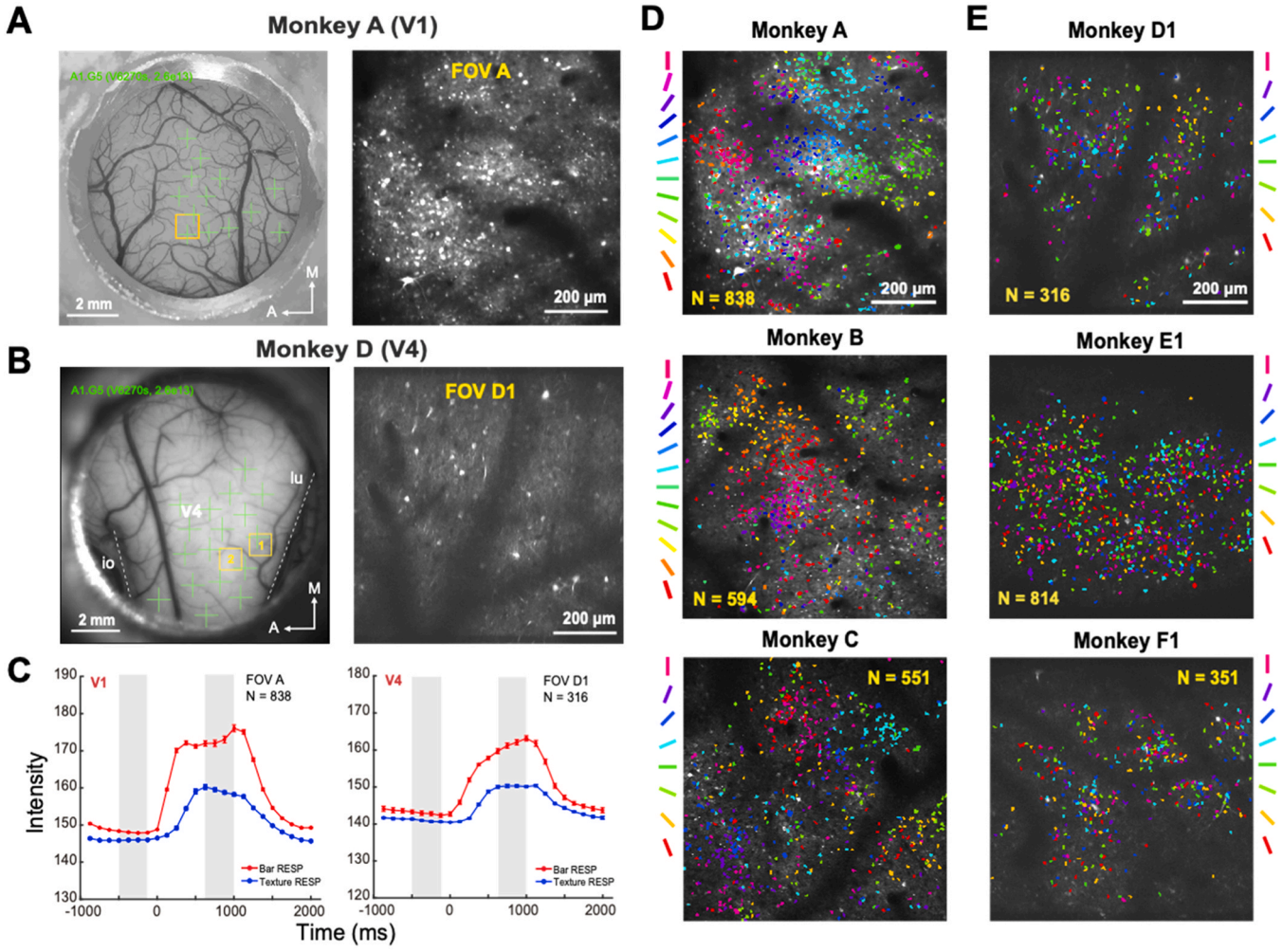

Fig. 1. Two-photon calcium imaging and orientation functional maps. A-B. Exemplar vascular maps (left) and average two-photon images of exemplar FOVs (850 × 850 μm^2) over a recording session (right) in V1 and V4, respectively. Green "+" signs indicate the viral injection regions. Yellow boxes on vascular maps indicate the FOVs chosen for two-photon imaging. A - anterior; M - medial; io - inferior occipital sulcus; lu - lunate sulcus. C. Exemplar time courses of calcium responses in V1 and V4. The red and blue curves are averaged over all orientation-tuned V1 or V4 neurons responding to the baseline conditions (a bar stimulus) and to various texture conditions, respectively. Each dot indicates the response intensity with one frame (8 fps after averaging every 4 frames). Error bars represent ±1 SEM. Shaded areas before or after the stimulus onset in each plot denote the 4 frames that were used for calculating the *F0* and *F* values, respectively. D. V1 orientation functional maps, each from one FOV of a macaque (Monkeys A-C). **E.** V4 orientation functional maps, each from one of two V4 FOVs of a macaque (Monkeys D-F).

surgery was performed 45 days later. A T-shaped steel frame was installed for head stabilization, and an optical window was inserted onto the cortical surface. Data collection could start as early as one week later. More details about the preparation and surgical procedures can be found in Li, Liu, Jiang, Lee, and Tang (Li et al., 2017). The procedures were approved by the Institutional Animal Care and Use Committee, Peking University.

2.2. Behavioral task

After a ten-day recovery period following the second surgery, monkeys were placed in a primate chair with head restraint. They were trained to hold fixation on a small white spot (0.2°) with binocular viewing. The eye positions were monitored by an Eyelink-1000 eye tracker (SR Research) at a sampling rate of 1000-Hz. During the experiment, trials with the eye position deviated 1.5° or more from the fixation before stimulus offset were discarded as ones with saccades and were repeated. For the remaining trials, the eye positions were mostly concentrated around the fixation point. We checked eye movements in one macaque (Monkey A). The eye tracker sampling rate was 1000 Hz, so it sampled 1000 times for each 1000-ms stimulus presentation per trial. A trial was regarded to have proper fixation when at least 500 samples of eye positions were within a radius of 0.50° from the central fixation. For a total of 288 trials with texture stimuli (24 conditions x 12 trials/condition), 274 (95.14 %) had proper fixation. Therefore, the reported results should not change significantly if a radius of 0.50° cutoff is used.

2.3. Visual stimuli and experimental design

Visual stimuli were generated with a Matlab-based Psychtoolbox-3 software (Pelli and Zhang, 1991) and presented on an Acer XB271HU monitor with a refresh rate of 80 Hz native, a resolution of 2560 pixel × 1440 pixel native, and a pixel size of 0.23 mm × 0.23 mm. The screen luminance was linearized by an 8-bit look-up table, and the mean luminance was 24 cd/m^2. The viewing distance was 60 cm.

A drifting square-wave grating with a spatial frequency of 4 cpd, a full contrast, a speed of 3 cycles/sec, a starting phase of 0°, and a size of 0.4° in diameter was used to determine the pRF location, shape, and approximate size associated with a specific response field of view (FOV). The same stimulus was also monocularly presented to confirm the V1 location as ocular dominance columns would appear. This fast process used a 4 × objective lens mounted on the two-photon microscope and did not provide cell-specific information. The recorded V1 pRF was centered at ~3.5° eccentricity in Monkey A, ~3.1° in Monkey B, and ~1.3° in Monkey C. All V1 pRFs were approximately circular in shape with a diameter of 0.9°. The recorded V4 pRFs were centered at 1.7°-1.9° in Monkey D, 2.6°-3.6° in Monkey E, and 0.5°-0.6° in Monkey F. V4 pRFs were elliptical in Monkeys D and E, with approximately 2.5° in height and 2° in width in two FOVs of Monkey D, and approximately 3° in height and 5° in width in two FOVs of Monkey E. In two FOVs of Monkey F, the V4 pRFs were circular, approximately 3° in both height and width (Fig. 3A).

The experimental texture stimuli were composed of oriented line segments with the same parameters as those in a previous study (Lamme, 1995; Poort et al., 2012). Two types of texture stimuli were used in the figure-ground experiment: the uniform texture and the figure-ground texture. The uniform texture was a 32° × 32° patch composed of randomly positioned line segments with two densities (0.05° × 0.2° segments at a density of 25 %, and 0.1° × 0.4° segments at a density of 16.7 %) at one of four orientations (0°, 45°, 90°, & 135°). The figure-ground texture was composed of a 4° × 4° square figure texture superimposed on a 32° × 32° uniform ground at the orthogonal orientation (Fig. 2A). To record neuronal responses to different texture positions, the figure texture was varied in five positions with V1 FOVs (0°, 1.5°, 2°, 2.5°, & 3°) and four positions with V4 FOVs (0°, 2°, 4°, & 6° for Monkeys D & F, and 0°, 2°, 4°, & 8° for Monkey E) relative to the pRF center of each FOV. All stimuli were viewed through a circular opening (diameter = ~28°) of a black cardboard covering the rest of the screen.

Each stimulus condition was presented for 1000 ms during recording, followed by an inter-stimulus interval (ISI) of 1500 ms that is sufficient to allow the calcium signals to return to the baseline level (Guan et al., 2018). Each stimulus condition was repeated 12 times. Imaging of neuronal responses to all pseudo-randomly presented stimulus conditions for a specific FOV and depth was completed in a single session that lasted 5–6 hours, during which monkeys had plenty of rest times.

2.4. Two-photon imaging

Two-photon imaging was performed using a Prairie Ultima IV (In Vivo) two-photon microscope (Prairie Technologies), along with a Ti: sapphire laser (Mai Tai eHP, Spectra Physics). GCaMP5 was chosen as the indicator of calcium signals because the fluorescence activities it expresses are linearly proportional to neuronal spike activities within a wide range of firing rates from 10 to 150 Hz (Li et al., 2017). During imaging, a 16 × objective lens (0.8 N.A., Nikon) with a resolution of 1.6 μm/pixel was used, along with a 1000-nm femtosecond laser. A fast resonant scanning mode (32 fps) was chosen to obtain continuous images of neuronal activities (8 fps after averaging every 4 frames). The strength of fluorescent signals (the luminance of a small area) was monitored and adjusted if necessary for drift of fluorescent signals. One or two response fields of view (FOVs) measuring 850 × 850 μm^2 were selected in each animal. Fig. 1 shows examples of the average two-photon images over a recording session at a V1 site in Monkey A (Fig. 1A) and a V4 site in Monkey D recording site 1 (Fig. 1B).

2.5. Data analysis: initial screening of ROIs

The data were analyzed using customized MATLAB codes. A normalized cross-correlation-based translation algorithm was used to correct motion artifacts (Li et al., 2017). After the correction, fluorescence changes were linked to corresponding visual stimuli through the time sequence information recorded by the Neural Signal Processor (Cerebus system, Blackrock Microsystem). By subtracting the mean of the 4 frames before the stimuli onset (*F0*) from the average of the *5th-8th* frames after the stimuli onset (*F*) across 12 repeated trials for the same stimulus condition, the differential image ($\Delta F = F - F0$) was obtained.

For V1 FOVs in Monkeys A-C, the regions of interest (ROIs) or possible cell bodies were determined through sequential analysis of 48 (Monkeys A-B) or 32 (Monkey C) differential images, in the order of 24 baseline conditions with a single bar at two lengths (2) and twelve orientations (12) for Monkeys A-B, or 8 baseline conditions with a single bar at eight orientations (8) for Monkey C, plus 24 texture conditions including 4 uniform texture conditions (4) and 20 figure-ground texture conditions (20). For six V4 FOVs in Monkeys D-F, ROIs were decided through sequential analysis of 60 differential images, in the order of 40 baseline conditions including a single bar at 8 orientations (8), and a single Gabor at 8 orientations (8) and 4 spatial frequencies (4) ($8 + 8 \times 4 = 40$), plus 20 texture conditions including 4 uniform texture conditions (4) and 16 figure-ground texture conditions (16).

More specifically, the 4 uniform texture conditions for both V1 and V4 FOVs included uniform textures composed of line segments at each of four orientations (0°, 45°, 90°, & 135°). The figure-ground texture patterns included 20 conditions for V1 FOVs, which were arranged in a 4 × 5 order, including 5 figure-pRF relative positions, and 4 texture line orientations. They also included 16 conditions for V4 FOVs, which were arranged in a 4 × 4 order, including 4 figure-pRF relative positions, and 4 texture line orientations.

To select ROIs, the differential images were filtered with a band-pass Gaussian filter (size = 2–10 pixels), and connected subsets of pixels (>25 pixels, which excluded smaller vertical neuropils) with the mean pixel

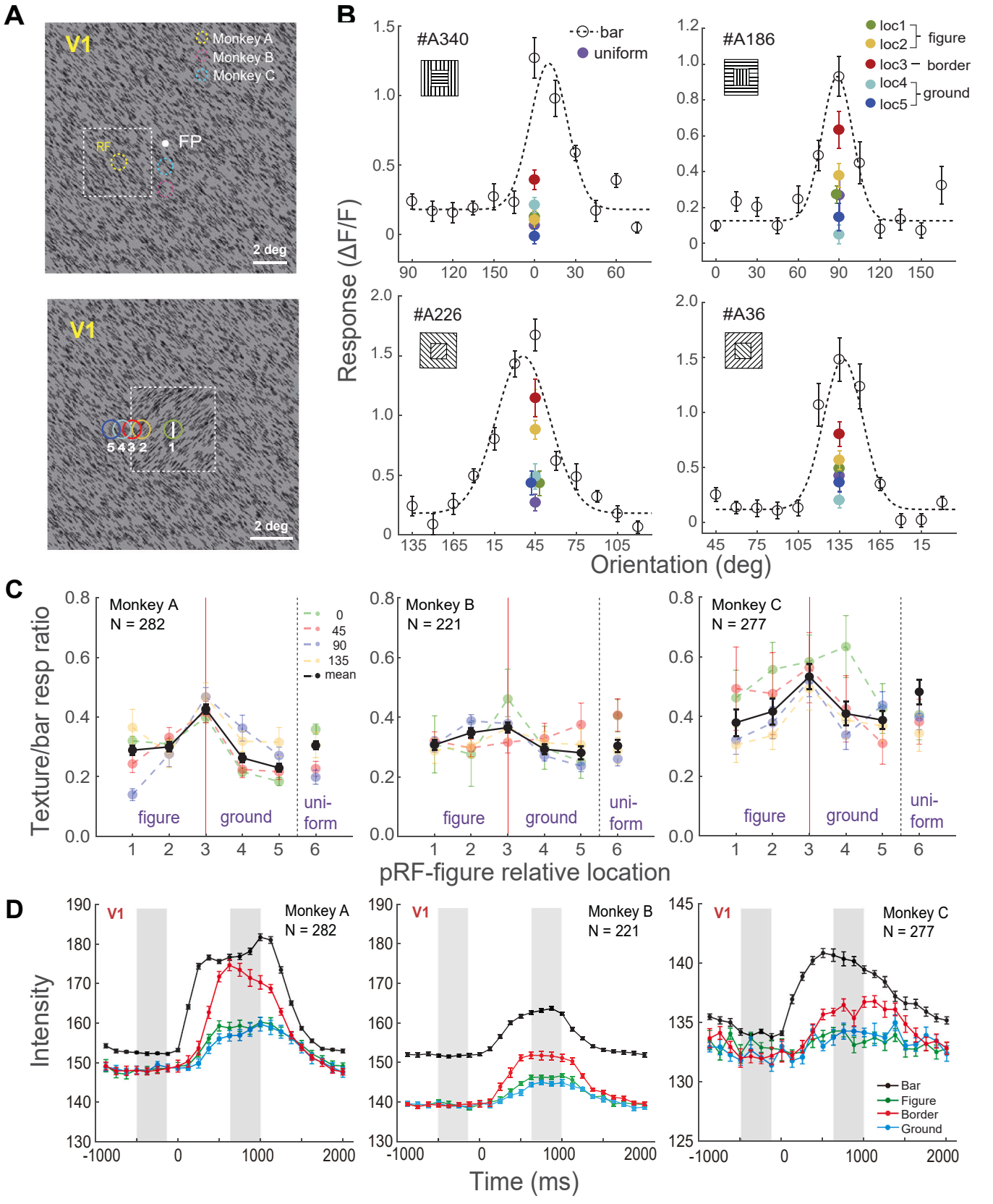

(caption on next page)

Fig. 2. Responses of V1 neurons to figure-ground texture stimuli. A. Stimuli. Upper: The exemplar figure-ground texture stimulus with a figure composed of 45° oriented line elements centered in the pRF of Monkey A FOV (yellow circle). The dotted color circles indicate the respective size and location of each pRF relative to the fixation point (FP). Lower: An enlarged view of five figure locations 0°, 1.5°, 2°, 2.5°, and 3° from the pRF. The white bar within loc1 (green circle) illustrates the relative size of the bar stimulus for baseline measurements. B. Four exemplar V1 neurons' orientation tuning functions with Gaussian fitting (open circles and dashed curves) and their responses to the figure-ground and uniform texture stimuli (filled circles). Error bars in this and other panels represent ±1 SEM. The top-left insets show the figure-ground texture stimuli with the figure at each neuron's preferred orientation. C. The mean texture/bar response ratios with the pRF located on loc1–5 of the figure-ground texture, and on the uniform texture. The colored lines (green, red, blue, and yellow) represent mean neuronal response ratios to textures at four texture line orientations, respectively, and the black lines indicate the grand means over four orientations. The vertical red lines indicate the texture border position (loc3). D. The time courses of calcium responses of V1 neurons tuned to the orientation of texture lines within the pRF. The colored lines indicate average fluorescence changes with the baseline (a bar stimulus), figure (loc1), border (loc3), and ground (loc5) conditions, respectively. The grey bars in each panel indicate the data points used in the calculations of calcium responses without and with the stimulus presentation.

value > 3 standard deviations of the mean brightness were selected as ROIs. Then the areas of these ROIs were set to mean brightness in the next differential image before the bandpass filtering and thresholding were repeated. This measure would eventually reduce the SDs of differential images and facilitate the detection of neurons with relatively low fluorescence responses. If a new ROI and an existing ROI from the previous differential image overlapped, the new ROI would be on its own if the overlapping area OA < 1/4 ROI_{new}, discarded if 1/4 ROI_{new} < OA < 3/4 ROI_{new}, and merged with the existing ROI if OA > 3/4 ROI_{new}. The merges would help smooth the contours of the final ROIs. This process went on twice through all differential images to select ROIs. Finally, the roundness for each ROI was calculated as:

$$Roundness = \frac{\sqrt{4\pi \times A}}{P}$$

where A was an ROI's area and P was the perimeter. Only ROIs with roundness larger than 0.9, which would exclude horizontal neuropils, were selected. No additional corrections for out-of-plane neuropil contamination was applied. Further analyses were based on the same ROIs with each FOV.

2.6. Imaging data analysis: selection of orientation-tuned neurons

The ratio of fluorescence change ($\Delta F/F0$) was calculated as a neuron's response to a specific stimulus condition. For a specific neuron's response to a specific stimulus condition, the $F0_n$ of the *n-th* trial was the average of 4 frames before stimulus onset (-500 – 0 ms), and F_n was the average of the *5th-8th* frames after stimulus onset (500–1000 ms). $F0_n$ was then averaged across 12 repeated trials to obtain the baseline F0 for all 12 trials (for the purpose of reducing noises in the calculation of responses), and $\Delta F_n/F0 = (F_n\text{-}F0)/F0$ was taken as the neuron's response to this stimulus at the *n-th* trial.

Several steps were taken to determine whether a neuron was orientation-selective. For a V1 neuron, we first selected the optimal bar length (0.15° × 0.89° or 0.15° × 1.22°) and the preferred orientation. Then, each neuron's responses to 12 (Monkeys A-B) or 8 (Monkey C) orientations at the optimal bar length over 12 repeats were compared by performing a non-parametric Friedman test to determine whether the neuron's responses at various orientations were significantly different from each other. For V4 neurons, we analyzed their neuronal responses to a center black bar (0.15° × 1.22° for Monkey D & F, and 0.15° × 1.56° for Monkey E) at 8 equal-spaced orientations. Each neuron's responses to 8 orientations over 12 repeats were also compared by a non-parametric Friedman test. The significance level was set at $\alpha = 0.05$ for both V1 and V4 neurons. Neurons passing the Friedman test were selected as orientation-tuned neurons and were used for later analysis, and each neuron's orientation preference was equal to the bar orientation that elicited the maximal mean response amplitude over 12 repeats.

2.7. Data analysis: principal component analysis (PCA)

To ensure consistent sample sizes of neuronal activities during linear-SVM training, we randomly selected 300 neurons each time for each FOV and applied principal component analysis (PCA) to their corresponding population response matrix $R \in R^{M\times N}$ to reduce dimensionality, where M was the number of recorded neurons ($M = 300$), and N ($N < M$) was the number of trials for all stimuli, including five types of texture (uniform, figure, border, and two ground locations), line elements at four orientations (0°, 45°, 90°, & 135°), and 12 repeated trials for each stimulus, leading to $N = 5 \times 4 \times 12 = 240$. This process was repeated 100 times to reduce the randomness brought by sampling. We implemented PCA through singular value decomposition (SVD):

$$R = \sum_{i=1}^{N} \sigma_i u_i v_i^T,\ (\sigma_1 \geqslant \sigma_2 \geqslant ... \geqslant \sigma_n)$$

where u_i was the i-th PC.

2.8. Data analysis: Linear classification and decoding

To assess the population decoding performance of V1 and V4 neurons, we trained the task-specific linear SVMs for each FOV using PCA-transformed neuronal responses.

For each task, we randomly selected 70 % of trials as the training set R_{train}, leaving the remaining 30 % as the testing set R_{test}. To assess the decoding performance with different principal components (PCs), we projected the neural codes to the first *1-j* PCs ($j \in$ [1:100]) to get the PCA-transformed neural responses V_{train} and V_{test}:

$$V_{train} = U_{1:j}^T R_{train}, \quad V_{test} = U_{1:j}^T R_{test},$$

where $U_{1:j} = [u_1, \ldots, u_j]$ were top j_{th} PCs extracted from the population response matrix. This process was repeated 100 times. Then a linear SVM was trained with the V_{train} and the corresponding labels Y_{train} for each classification task. The objective function was:

$$\underset{w,b}{arg\min} \frac{2}{||w||}, \qquad s.t. \quad Y_{train_i}\left(w^T V_{train_i} + b\right) > 1.$$

After obtaining discrimination weight vector w and discrimination offset b, the decoding accuracy Acc on the test set V_{test} and the corresponding labels Y_{test} was calculated:

$$Acc = \frac{\sum_{i=1}^{[N\times 0.3]} count((w^T V_{test\,i} + b) \quad \times \quad Y_{test\,i})}{[N \times 0.3]},$$

where $count(x) = 1$ when $x > 1$, otherwise $count(x) = 0$, and $[\bullet]$ was the rounding operator. Since the objective function was non-convex, this process was repeated ten times and the highest accuracy was used for each task.

To assess how individual neurons were weighted in the linear discriminant analysis during figure-ground decoding, we calculated the neuronal decoding weight vector D_{train} by mapping the population decoding weight vector of the top j_{th} PCs on the training set back to each neuron:

$$D_{train} = U_{1:j} w$$

Where D_{train} was the neuronal decoding weight vector averaged across

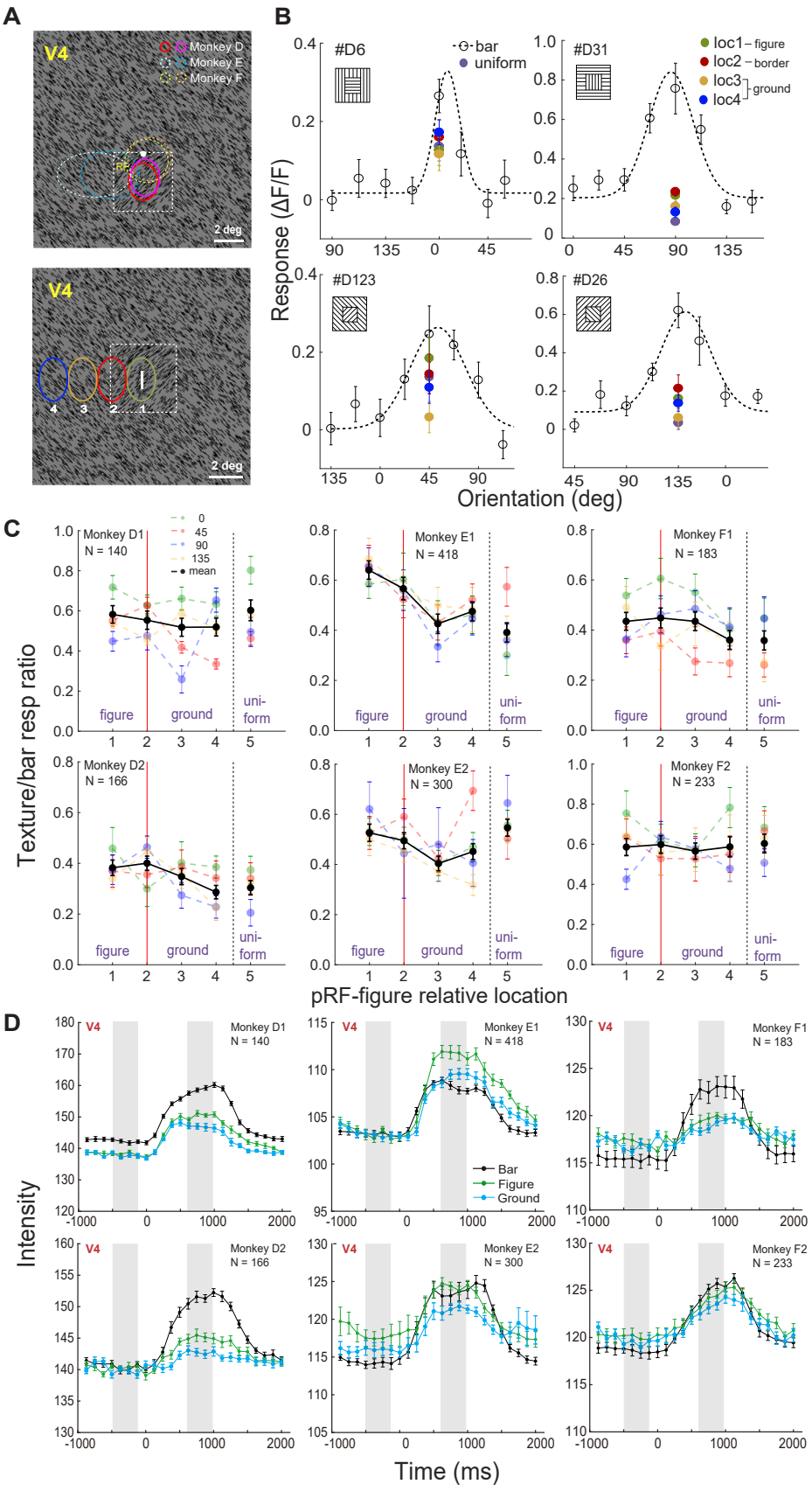

(caption on next page)

Fig. 3. Responses of V4 neurons to figure-ground texture stimuli. A. Stimuli. Upper: An exemplar figure-ground texture stimulus with the figure containing 45° oriented lines centered in the pRF of Monkey D1 FOV (red circle). The dotted color circles indicate the sizes and locations of pRFs in six V4 FOVs relative to the fixation point (FP). Lower: An enlarged view of V4 pRF locations related to the figure, which were 0°, 2°, 4°, or 6° from the figure center. The white bar in loc1 indicates the relative size of the black bar used in V4 experiments as the baseline condition. B. Four exemplar V4 neurons' orientation tuning functions with Gaussian fitting and their responses to loc1–4 of the figure-ground texture and the uniform texture. Error bars in this and other panels represent ±1 SEM. The top-left insets show the figure-ground texture stimuli with the figure at each neuron's preferred orientation. C. The mean texture/bar response ratios with pRF located at loc1–4 of the figure-ground texture stimulus and on the uniform texture. The colored dots and lines (green, red, blue, and yellow) represent mean neuronal texture/bar response ratios to textures at four texture line orientations, respectively, and the black dots and lines indicate the mean values averaged across four orientations. D. The time courses of calcium responses of V4 neurons tuned to the orientation of texture lines within the pRF. The colored lines indicate average fluorescence changes responding to the baseline (a bar stimulus), texture figure (loc1), and ground (loc4) conditions, respectively. The grey bars in each panel indicate the data points used in the calculations of calcium responses without and with the stimulus presentation.

100 bootstraps, $U_{1:j} = [u_1, \ldots, u_j]$ were the top j_{th} PCs of PCA-transformed neuronal responses, and w was the discrimination weight vector.

2.9. Experimental design and statistical analyses

Mixed-design ANOVAs were performed for data presented in Figs. 2 and 3. A Huynh-Feldt correction was applied if Mauchly's Test of sphericity was violated.

3. Results

V1 neuronal responses for figure-ground texture segregation were measured in three FOVs, one in each macaque (Fig. 1A). All three V1 FOVs were located 150–200 μm deep from the cortical surface, centered at an eccentricity of approximately 3.5° in Monkey A, 3.1° in Monkey B, and 1.3° in Monkey C. V4 neuronal responses were measured in three additional macaques (D-F), with two FOVs in each macaque (Fig. 1B). All six V4 FOVs situated 150–300 μm deep from the cortical surface, centered at an eccentricity of approximately 1.7°-1.9° in Monkey D, 2.6°-3.6° in Monkey E, and 0.5°-0.6° in Monkey F. A total of 1983 V1 neurons (77.9 % of all identified V1 neurons) and 2820 V4 neurons (54.4 % of all identified V4 neurons) were classified as orientation-tuned neurons (more details provided in Table S1). These neurons were included in the data analysis.

3.1. V1 neuronal responses to figure-ground texture stimuli

We first recorded the responses of V1 superficial-layer neurons to figure-ground texture stimuli. The figure-ground textures consisted of a 4° × 4° figure embedded in a 32° × 32° ground, consistent with those used by Lamme (Lamme, 1995). The figure was formed by iso-oriented lines at one of four orientations (0°,45°,90°, and 135°), and the ground was comprised of lines orthogonal to the figure lines (Fig. 2A). The stimulus was positioned relative to the population receptive field (pRF) of a FOV (see Materials and Methods), such that the figure (loc1–2), vertical figure-ground border (loc3), and ground (loc4–5) fell on the pRF, respectively. The texture stimulus was regenerated every trial (only the figure texture was refreshed to save the computing time) at one of four orientation combinations in a random order. It was presented randomly in one of five locations, along with four uniform textures (figure and background lines oriented identically) at four orientations. Additionally, responses to a single bar stimulus at various orientations were assessed separately in the same session as baselines.

Fig. 2B depicts the orientation tuning functions of four exemplar neurons from Monkey A measured with an oriented bar and their Gaussian fittings. The figure also portrays their responses to the figure-ground texture at different positions relative to the pRF, as well as to the uniform texture, when the texture line elements in pRF aligned with their preferred orientations. Compared to the peak of the orientation tuning function, there was an overall suppression in the neuronal responses to the texture. Nonetheless, a lesser degree of suppression was evident when the border of the figure-ground texture (loc3) coincided with the pRF.

The same pattern was observed in terms of average response changes in all three monkeys. Fig. 2C summarizes the mean ratios of neuronal responses to various texture conditions over those to respective optimal bars (texture/bar response ratios) at four texture orientations (0°, 45°, 90°, & 135°) and the grand means. The analysis presented below used four groups of neurons, each tuned to one of four texture line orientations (0°, 45°, 90°, & 135°), for the purpose of testing whether the effects were invariant to the orientation preferences of participating neurons. Additional analysis based on all orientation-tuned neurons in each FOV is presented in Fig. S1. During data analysis (ANOVA below and with Fig. S1), the figure and ground responses by the same neurons were compared when the orientation of figure and ground line elements in pRF was identical (i.e., figure and ground were from different texture stimuli), which would ensure that the pRF was stimulated by the same local features (Lamme, 1995). However, the figure-ground border formed by abutting orthogonal line elements was a composite stimulus, the potential impact of which will be discussed in the Discussion.

A mixed-design ANOVA was conducted to analyze these data with Location (loc1–5 and the uniform texture) as a within-subject factor, and Orientation Preference (0°, 45°, 90°, & 135°) and Monkey as between-subject factors. The ANOVA outputs revealed significant main effects of Location ($F_{5,\ 3870} = 12.468$, $p < 0.001$, $\eta_p^2 = 0.016$) and Monkey ($F_{2,\ 774} = 15.790$, $p < 0.001$, $\eta_p^2 = 0.039$), but no significant main effect of Orientation Preference ($F_{3,\ 774} = 0.609$, $p = 0.610$, $\eta_p^2 = 0.002$).

When analyzed individually (the same ANOVA without Monkey as a between-subject factor), the main effect of Location was significant in Monkey A ($F_{5,\ 1390} = 31.925$, $p < 0.001$, $\eta_p^2 = 0.103$) and Monkey C ($F_{5,\ 1365} = 2.432$, $p = 0.042$, $\eta_p^2 = 0.009$), and marginally significant in Monkey B ($F_{5,\ 1085} = 2.094$, $p = 0.068$, $\eta_p^2 = 0.010$). Planned contrast analysis further indicated that the neuronal responses to the figure-ground border (loc3) were significantly higher than those to the other four locations in each monkey ($p_A < 0.001$, $p_B = 0.005$, and $p_C = 0.004$). In addition, there was no significant difference between responses to the figure center (loc1) and the background (loc5) ($p_A = 0.245$, $p_B = 0.660$, and $p_C = 0.846$). These results, as well as similar ones when all orientation-tuned neurons were considered (Fig. S1) align more closely with Rossi et al. (2001), in that V1 neurons are more likely to detect the figure-ground texture border rather than distinguishing the figure from the ground. The effects are also appreciable through a large portion of the calcium response time courses with each FOV (Fig. 2D). Notably, orientation-untuned neurons also exhibited similar but weaker effects (Fig. S2), which we will explore in a separate study.

3.2. V4 neuronal responses to figure-ground texture stimuli

The same figure-ground texture stimuli were used here for V4 recording. The heights of pRFs from Monkeys D were approximately 63 % of the figure's height, while those from Monkeys E and F were about 75 % of the figure's height (Fig. 3A upper panel). During the experiments, the center of the figure texture was varied in four positions relative to the pRF center in a step of 2° (loc1–4, Fig. 3A lower panel). Fig. 3B displays the orientation tuning functions of four exemplar V4 neurons from Monkey D, as well as their responses to a uniform texture and figure-ground textures at various pRF-relative locations. Similar to

observations in V1 (Fig. 2B), neuronal responses to the texture stimuli were suppressed compared to the peak bar responses. However, there was no consistent trend observed in responses to loc1–4.

Fig. 3C summarizes the mean texture/bar response ratios at four texture line orientations (0°, 45°, 90°, & 135°) and the grand means. A mixed-design ANOVA analyzed these data with Location (loc1–4 & the uniform texture) as the within-subject factor, and Orientation Preference and Monkey as between-subject factors. The results indicated significant main effects of Location ($F_{4,\ 5724} = 5.407$, $p < 0.001$, $\eta_p^2 = 0.004$), and Monkey ($F_{5,\ 1431} = 8.847, p < 0.001, \eta_p^2 = 0.030$), while the main effect of Orientation Preference was insignificant ($F_{3,\ 1431} = 1.686$, $p = 0.168$). Further planned contrast analysis revealed that neuronal responses to the figure and the border (loc1–2) were significantly higher than those to the background (loc3–4) in FOVs D2, E1, and E2 ($p_{D2} = 0.021$, $p_{E1} < 0.001$, and $p_{E2} = 0.024$), but not in other three FOVs ($p_{D1} = 0.119$, $p_{F1} = 0.179$, and $p_{F2} = 0.591$). The effects can also be seen in time courses of fluorescence signals with each FOV (Fig. 3D). Similar effects were also evident when responses of all orientation-selective neurons for each FOV were analyzed (Fig. S3). These results are largely consistent with previous findings regarding V4 involvement in figure-ground texture segregation (Poort et al., 2012; Poort et al., 2016). They also receive further support from the population coding analysis below.

3.2.1. V1 and V4 population coding for figure-ground texture segregation

To delve deeper into the roles of V1 and V4 neurons in figure-ground texture segregation, particularly because the ANOVA results of average responses showed very small effect sizes and significant variations among animals/FOVs, we utilized a machine-learning approach to explore their population coding properties. First, we conducted principal component analysis (PCA) to reduce the dimensionality of the population responses of all orientation-tuned neurons within each FOV. We then used linear Support Vector Machines (SVMs) trained on PCA-transformed data to execute figure-ground texture segregation in two classification tasks (Materials and Methods). Specifically, for each FOV, we first trained the linear SVM to distinguish the figure-ground border from the other three texture conditions (border vs. figure/ground/uniform textures). Then we trained the linear SVM to differentiate the figure from the ground (figure vs. background), during which the classifier learned to discern whether the neurons' pRF lay inside or outside the figure. These procedures were repeated with feature-label shuffled data for comparisons.

Fig. 4A displays the average decoding accuracies for 1–100 principal components (PCs) of neuronal population activities from three V1 and six V4 FOVs in two classification tasks. Decoding accuracy of 75 % or higher was achieved in both tasks in V1 and V4 with an adequate number of PCs, in contrast to around 50 % chance accuracy with

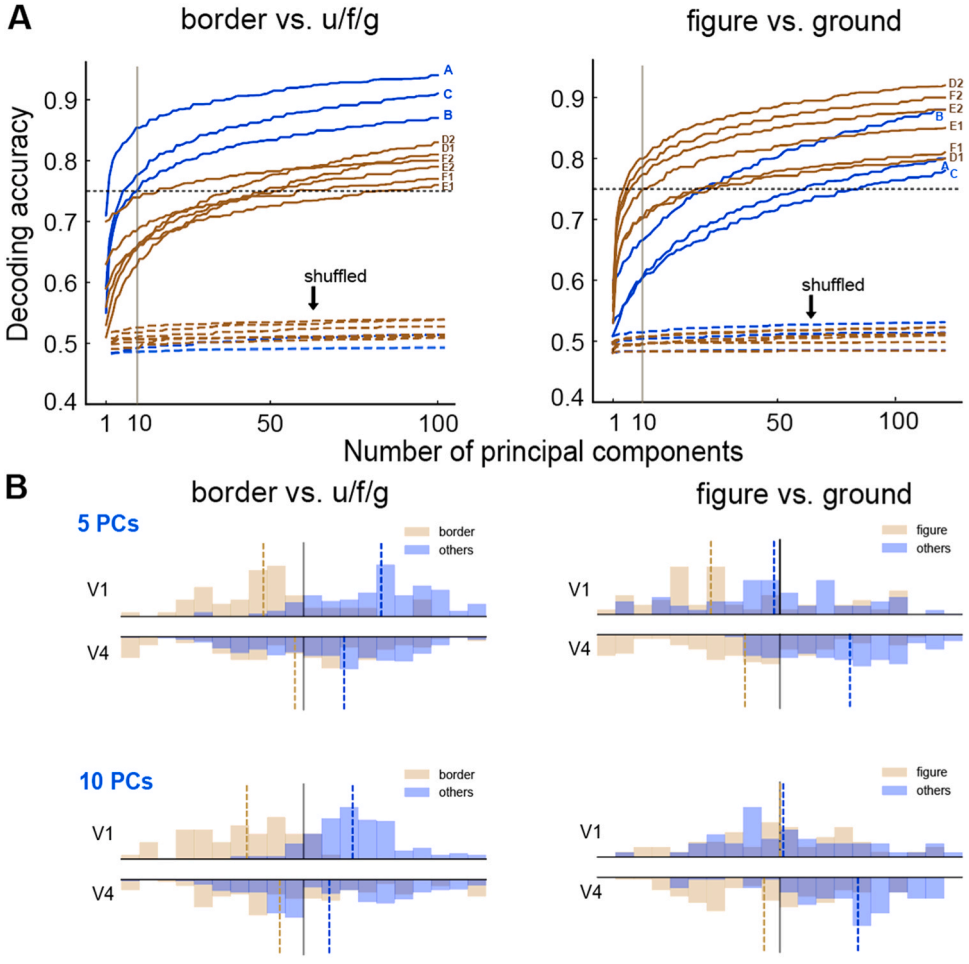

Fig. 4. Population coding of figure-ground texture stimuli by V1 and V4 neurons. A. The respective decoding accuracies for two SVM tasks (border vs. uniform/figure/ground textures and figure vs. ground) as a function of the number of principal components. The solid curves represent the average decoding accuracies in each of the three V1 FOVs (blue) from Monkeys A-C and six V4 FOVs (red) from Monkeys D-F. The dashed curves represent corresponding decoding accuracies with shuffled data. The black horizontal lines indicate 75 % decoding accuracy. B. The upper and lower panels show the histograms of V1 and V4 normalized projection values when using the top 5 PCs and 10 PCs to train the linear SVMs for two classification tasks, respectively. The black solid lines in each panel indicate the decision boundary (projection value = 0) and colored dashed lines indicate the median projection values of two classes of testing features for each task. In the bottom-right panel (10 PCs, figure vs. ground), the V1 projection values with 10 PCs overlapped, so only one dashed vertical line is visible.

shuffled data. This suggests that texture information could be encoded by both V1 and V4 neurons and readout linearly. However, there were dramatic differences in decoding efficiencies between V1 and V4 neurons across tasks. V1 neurons decoded figure-ground texture borders more efficiently, reaching 75 % accuracy with an average of 6 PCs over FOVs of Monkeys A-C, in contrast to the 50 PCs averaged over V4 FOVs of Monkeys D-F. This indicates that the border information is well represented in the first few most informative PCs by V1 neurons. On the other hand, V4 neurons were more efficient in decoding the figure from the ground, requiring 13 PCs in V4 as opposed to 49 PCs in V1 to reach 75 % accuracy, suggesting that figure-ground information is poorly structured in V1 neurons than in V4 neurons.

For easy visualization of the results, we additionally calculated the projection values, which represent the distances (normalized to [-1,1]) between the decision boundary and the testing features (i.e., PCA-transformed neuronal responses in the testing dataset). Fig. 4B presents the histograms of projection values in V1 and V4 for each classification task when the top 5 PCs (upper panels) and 10 PCs (lower panels) were used to train the linear SVMs. When segregating the border from other textures (i.e., uniform, figure, and ground), V1 outperformed V4 as judged by the distance from the median projection values of the two classes of features to the decision boundary. However, V1 could not differentiate the figure from the ground with 5 and 10 PCs, whereas V4 could achieve figure-ground segregation even with only 5 PCs.

For simplicity, the above decoding procedure used a single set of decoding weights for each FOV to differentiate each texture condition (e.g. border vs. figure/ground/uniform textures and figure vs. ground), regardless of the texture line orientations. When separate linear SVM decoders were developed for textures composed of lines with different orientation pairs (0° & 90° and 45° & 135°), decoders trained with V1 neurons tuned to all orientations exhibited better performance than those trained with V1 neurons preferring texture-line orientations or other orientations for decoding border vs. figure/ground/ uniform textures (Fig. S4). This difference was not shown in V4 neurons. Furthermore, decoders trained with neurons tuned to all orientations, to texture-line orientations, and to other non-texture line orientations displayed similar performance for decoding figure vs. ground in both V1 and V4 (Fig. S4).

We then examined the relationship between figure-ground population decoding and the response characteristics of individual neurons. The contribution of each neuron to figure-ground decoding was quantified by calculating normalized decoding weights for 5, 10, 20, and 40

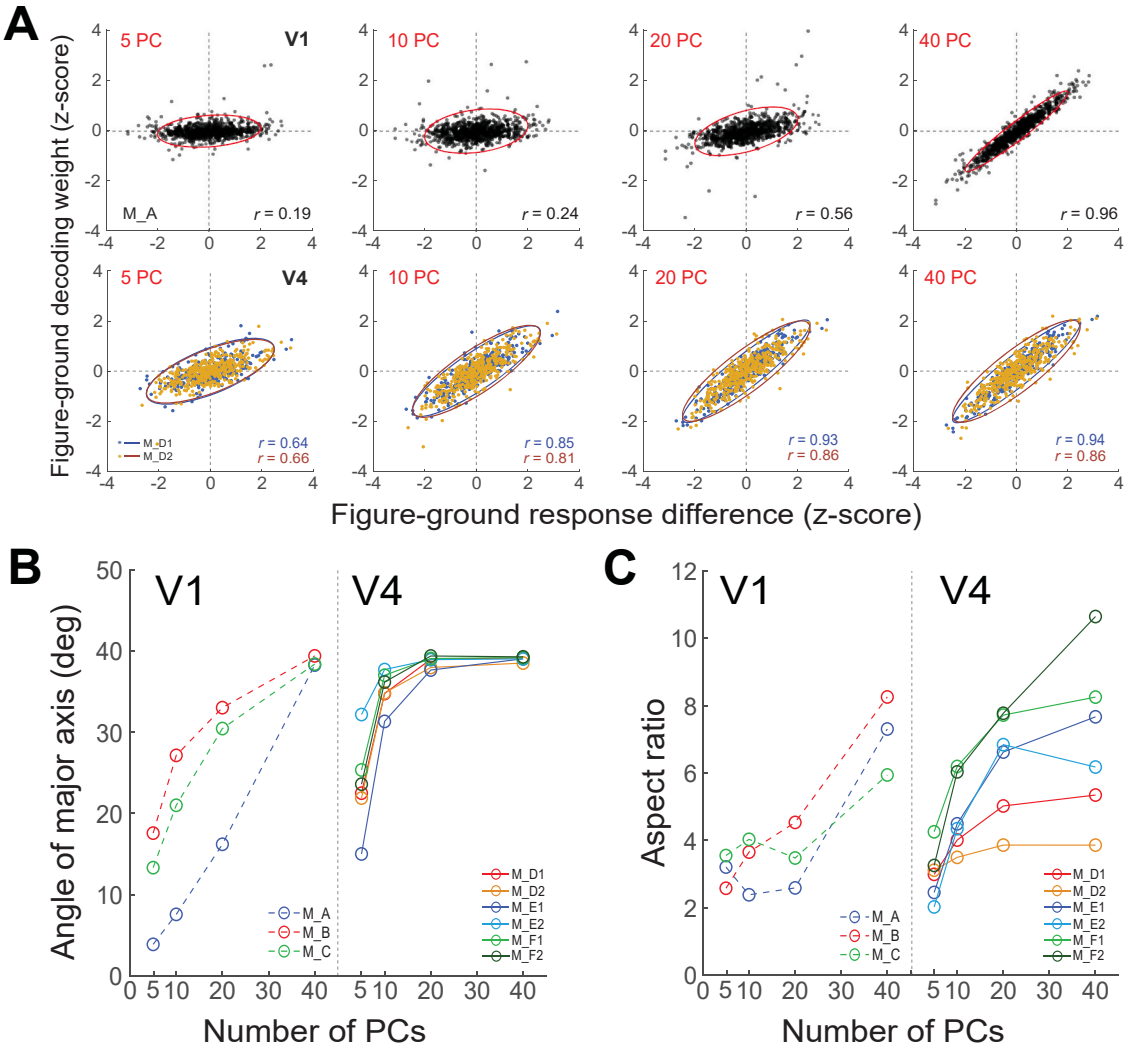

Fig. 5. The relationship between figure-ground decoding weights and figure-ground response differences in V1 and V4 neurons. A. Distributions of figure-ground decoding weights plotted against figure-ground response differences of individual neurons in V1 and V4, using 5, 10, 20, and 40 PCs in exemplar FOVs. Each data point represents one neuron. An ellipse is depicted in each plot to represent the statistical distribution of decoding weights and neuronal response differences, with a cutoff of ±1.5 standard deviations. The horizontal zero line indicates zero contribution. B. Analysis of the angles between the major axis of the ellipses and the x-axis with 5, 10, 20, and 40 PCs for all FOVs in V1 and V4. C. Comparisons of aspect ratios of the ellipses with 5, 10, 20, and 40 PCs in V1 and V4 FOVs.

PCs (see Materials and Methods). These decoding weights under four PC conditions were contrasted to the neuron's figure-ground response difference, calculated as the difference between responses to the figure center (loc1) and the ground (loc5 for V1 neurons and loc4 for V4 neurons) at the matching texture line orientation (Fig. 5A).

In Fig. 5A, the upper and lower panels display outcomes from an exemplar V1 FOV (Monkey A) and two exemplar V4 FOVs (Monkey D1-D2), respectively. The neuronal data distributions are depicted using ellipses, where the major and minor axes represent the eigenvectors of the covariance matrix of figure-ground decoding weights and neuronal figure-ground response differences. The angle between the major axis of the ellipse and the x-axis, akin to the slope of a linear regression line, suggests how much the change in the response difference predicts the variation in decoding weight. A wider angle signifies a greater influence of the response difference on figure-ground decoding. The aspect ratio of the ellipse reflects the covariance structure between decoding weights and neuronal response differences. A higher aspect ratio implies that individual neurons are more precisely weighted during figure-ground decoding, potentially indicating improved sensitivity or decoding accuracy. Compared to V4 neurons, the figure-ground response difference of V1 neurons showed less predictive capability for their contributions to figure-ground decoding and exhibited lower decoding accuracy with up to 20 PCs. In contrast, V4 neurons displayed greater predictive capability with a relatively small number of PCs. Similar trends were observed in other FOVs (Fig. 5B-C). These findings are consistent with earlier PCA data (Fig. 4), indicating poor figure-ground decoding by V1 neurons unless a significant number of PCs are considered. Moreover, the figure-ground decoding at the population level was primarily driven by neurons with larger figure-ground response differences.

Aside from these findings, we found no significant relationships between figure-ground decoding weights and orientation-tuning properties (e.g., orientation preference and bandwidth) or the spatial distributions of orientation-tuned neurons (Figs. S5-S7). This could be attributed to the abstract response dimensions identified through PCA, which makes it difficult to trace the decoding contributions of neurons back to their specific RF properties.

4. Discussion

Texture-based figure-ground segregation involves three complementary processes: border detection, region-filling, and background suppression (Lamme et al., 1999; Poort et al., 2012; Poort et al., 2016; Self et al., 2013). The current study primarily focuses on the first two processes. The average response changes suggest that V1 neurons mainly detect the texture border, rather than segregate the figure from the ground. However, population data analysis shows that V1 neurons also play a role in figure-ground decoding, albeit less efficiently, as the figure-ground information is not well-represented in the first and most informative principal components of population responses. Together, these results suggest that V1 neurons are primarily responsible for figure border detection, and the poorly structured figure-ground information they carry may be utilized by V4 neurons to accomplish figure-ground segregation. These findings help reconcile previous debates from a new population perspective on the roles of V1 and V4 neurons in figure-ground texture segregation.

On the other hand, population data analysis confirms that V4 neurons can effectively represent figure-ground information using only a few principal components. The contributing neurons are those with higher absolute figure-ground response differences, as evidenced by the strong correlations between figure-ground decoding weights and figure-ground response differences. As V1 neurons are more adept at defining the figure border, V4 neurons may "fill" the figure region outlined by these borders. This process may also involve top-down signals from higher brain areas like V4, FEF, and DLPFC (Super et al., 2001; Poort et al., 2012; Poort et al., 2016; Huang et al., 2020). Even under passive viewing, the orientation contrasts of texture lines in the texture stimuli may be salient enough to capture attention. Therefore, our results are not immune to modulation from top-down signals.

Our findings indicate that the detection of second-order texture borders is not dependent on the orientation tuning of V1 neurons responding to first-order luminance lines (Fig. 2C). In fact, many V1 neurons can be activated by both first-order and second-order oriented stimuli, often with different preferred orientations (El-Shamayleh and Movshon, 2011; Ju et al., 2022). Therefore, it is possible that the detection of texture borders involves V1 neurons whose second-order orientation preferences match the texture border orientation, while their first-order orientation preferences align with the orientation of the texture line elements. Previous electrode recording studies found limited participation of V1 neurons in detecting second-order orientation when the latter were defined by contrast envelopes made by multiplication of a low-spatial frequency grating (as the envelope) and a high-spatial frequency grating (as the carrier) of different orientations (Zhou and Baker, 1994; El-Shamayleh and Movshon, 2011; Li et al., 2014). However, two overlapping gratings at different orientations would induce cross-orientation suppression, which may explain the weak evidence for V1's role in second-order orientation processing in those studies.

It is challenging to offer an explanation why our two-photon calcium results are in discrepancy from some but not all of the previous electrode recording studies regarding the roles of V1 neurons in figure-ground texture segregation. Two-photon imaging offers the advantage of sampling a large quantity of neurons with fewer sampling biases compared to electrode recordings. It certainly has its limitations too. For example, calcium signals are much slower than spiking activities, and the aggregated calcium responses over a long period (e.g., 1000 ms in the current study) could obscure the brief spike responses to the texture. Moreover, calcium signals may exaggerate the nonlinear properties of neurons, even if calcium signals indicated by GCaMP5, our preferred calcium indicator, display a linear relationship to neuronal spike rates within a range of 10–150 Hz (Li et al., 2017). Nonetheless, these limitations shall have affected the V1 responses under all texture conditions, yet stronger responses to texture borders were distinct, and figure responses were not consistently stronger than ground responses among FOVs. In a mice calcium imaging study, V1 neurons indeed exhibited stronger figure activities than ground activities (Kirchberger et al., 2021). However, results from mice studies may not be applicable to the macaque visual cortex because of the huge inter-species differences. On the other hand, population coding analysis indicates that V1 neurons indeed contribute to figure-ground texture decoding. This contribution is mainly from neurons with larger positive or negative figure-ground responses differences when many principal components are involved to represent poorly structured figure-ground information. Because positive and negative response differences cancel each other out, statistical analysis comparing average responses cannot reveal these contributions.

Finally, several technical notes: First, there were variations in responses among different animals, as a significant main effect of Monkey was suggested by ANOVA for both V1 and V4 texture responses. In addition, the orientation preferences of neurons were not evenly distributed within and across FOVs (Table S1). One theoretically simple but practically challenging solution is to increase the number of participating animals and FOVs. Increasing the size of FOVs is another technically demanding solution. Nevertheless, population coding results exhibit greater consistency among animals (Figs. 4 and 5). In particular, in Fig. 5, a small subset of the most relevant neurons received higher weights to encode task-related texture features, while the majority received lower weights. In contrast, conventional statistical methods implicitly assume equal weights for all neurons regardless of their relevance, which would lead to larger variations among animals and stimulus conditions.

Secondly, we employed a population RF approach and did not measure the exact RF of each ROI. However, the identified neurons most likely had their RFs overlapping with the stimulus, resulting in significant responses. A recent two-photon imaging study (Nauhaus et al.,

2016) reported that the RF scatter in V1 was approximately half of the originally estimate by Hubel and Wiesel (1974). Our own detailed RF mapping data (unpublished) also suggest that the RF scatters of superficial-layer V1 neurons have very narrow distributions (vertical and horizontal standard deviations both $< 0.15°$). Hence, our measurements likely captured most neurons that could be triggered by the stimuli. There may have been some neurons whose RFs did not align well with the stimulus and thus exhibited weak and orientation-unspecific responses. These neurons would have been filtered out through data analysis (see Materials and Methods).

Thirdly, the pRFs of two FOVs in Monkey E V4 were situated in the lower-left region of the visual field, with an eccentricity of 2.6–3.6°. During the experiment, as the figure was horizontally shifted from left to right (from loc1 to loc4), it initially approached the fovea and then moved away, as illustrated in Fig. S8. These location changes triggered a significant figure enhancement effect akin to other FOVs. Therefore, the horizontal displacement of the texture stimulus in the V4 experiment (Fig. 3) did not correspond to a reduction in retinal eccentricity, and the changes of neuronal responses were not caused by retinal eccentricity alternations.

CRediT authorship contribution statement

Xing-Nan Zhao: Writing – original draft, Formal analysis, Data curation. **Xing-Si Dong:** Writing – original draft, Visualization, Formal analysis. **Dan Qing:** Data curation. **Si Wu:** Writing – review & editing. **Shi-Ming Tang:** Writing – review & editing, Methodology. **Cong Yu:** Writing – review & editing, Writing – original draft, Formal analysis, Conceptualization.

Declaration of competing interest

None.

Data Availability

Data will be made available on request.

Acknowledgments

This study was supported by a Ministry of Science and Technology, China, STI2030-Major Projects grant (2022ZD0204600), Natural Science Foundation of China grants 31230030 and 31730109, and funds from Peking-Tsinghua Center for Life Sciences, Peking University.

Appendix A. Supporting information

Supplementary data associated with this article can be found in the online version at doi:10.1016/j.pneurobio.2024.102655.

References

El-Shamayleh, Y., Movshon, J.A., 2011. Neuronal responses to texture-defined form in macaque visual area V2. J. Neurosci. *31*, 8543–8555.
Guan, S.C., Zhang, S.H., Zhang, Y.C., Tang, S., Yu, C., 2018. Plaid detectors in macaque V1 revealed by two-photon calcium imaging. Curr. Biol. *30*, 934–940.
Guan, S.C., Ju, N., Tao, L., Tang, S.M., Yu, C., 2021. Functional organization of spatial frequency tuning in macaque V1 revealed with two-photon calcium imaging. Prog. Neurobiol. *205*, 102120.
Huang, L., Wang, L.J., Shen, W.M., Li, M.S., Wang, S.Y., Wang, X.T., Zhang, X.L., 2020. A source for awareness-dependent figure-ground segregation in human prefrontal cortex. Proc. Natl. Acad. Sci. USA *117*, 30836–30847.
Hubel, D.H., Wiesel, T.N., 1974. Uniformity of monkey striate cortex: a parallel relationship between field size, scatter, and magnification factor. J. Comp. Neurol. *158*, 295–305.
Ju, N., Guan, S.C., Tao, L., Tang, S.M., Yu, C., 2021. Orientation tuning and end-stopping in macaque V1 studied with two-photon calcium imaging. Cereb. Cortex *31*, 2085–2097.
Ju, N.S., Guan, S.C., Tang, S.M., Yu, C., 2022. Macaque V1 responses to 2nd-order contrast-modulated stimuli and the possible subcortical and cortical contributions. Prog. Neurobiol. *217*, 102315.
Julesz, B., 1981. A theory of preattentive texture-discrimination based on 1st-order statistics of textons. Biol. Cybern. *41*, 131–138.
Kirchberger, L., Mukherjee, S., Schnabel, U.H., van Beest, E.H., Barsegyan, A., Levelt, C. N., Roelfsema, P.R., 2021. The essential role of recurrent processing for figure-ground perception in mice. Sci. Adv. *7*.
Lamme, V.A.F., 1995. The neurophysiology of figure ground segregation in primary visual-cortex. J. Neurosci. *15*, 1605–1615.
Lamme, V.A.F., Rodriguez-Rodriguez, V., Spekreijse, H., 1999. Separate processing dynamics for texture elements, boundaries and surfaces in primary visual cortex of the macaque monkey. Cereb. Cortex *9*, 406–413.
Li, G., Yao, Z., Wang, Z., Yuan, N., Talebi, V., Tan, J., Baker, C.L., Jr, 2014. Form-cue invariant second-order neuronal responses to contrast modulation in primate area V2. J. Neurosci. *34*, 12081–12092.
Li, M., Liu, F., Jiang, H., Lee, T.S., Tang, S., 2017. Long-term two-photon imaging in awake macaque monkey. Neuron *93*, 1049–1057 e1043.
Marcus, D.S., Van Essen, D.C., 2002. Scene segmentation and attention in primate cortical areas V1 and V2. J. Neurophysiol. *88*, 2648–2658.
Merigan, W.H., 1996. Basic visual capacities and shape discrimination after lesions of extrastriate area V4 in macaques. Vis. Neurosci. *13*, 51–60.
Nauhaus, I., Nielsen, K.J., Callaway, E.M., 2016. Efficient receptive field tiling in primate V1. Neuron *91*, 893–904.
Pelli, D.G., Zhang, L., 1991. Accurate control of contrast on microcomputer displays. Vis. Res *31*, 1337–1350.
Poltoratski, S., Maier, A., Newton, A.T., Tong, F., 2019. Figure-ground modulation in the human lateral geniculate nucleus is distinguishable from top-down attention. Curr. Biol. *29*, 2051–2057 e2053.
Poort, J., Raudies, F., Wannig, A., Lamme, V.A., Neumann, H., Roelfsema, P.R., 2012. The role of attention in figure-ground segregation in areas V1 and V4 of the visual cortex. Neuron *75*, 143–156.
Poort, J., Self, M.W., van Vugt, B., Malkki, H., Roelfsema, P.R., 2016. Texture segregation causes early figure enhancement and later ground suppression in areas V1 and V4 of visual cortex. Cereb. Cortex *26*, 3964–3976.
Rossi, A.F., Desimone, R., Ungerleider, L.G., 2001. Contextual modulation in primary visual cortex of macaques. J. Neurosci. *21*, 1698–1709.
Self, M.W., van Kerkoerle, T., Super, H., Roelfsema, P.R., 2013. Distinct roles of the cortical layers of area V1 in figure-ground segregation. Curr. Biol. *23*, 2121–2129.
Super, H., Spekreijse, H., Lamme, V.A.F., 2001. Two distinct modes of sensory processing observed in monkey primary visual cortex (V1). Nat. Neurosci. *4*, 304–310.
Zhou, Y.X., Baker, C.L., Jr, 1994. Envelope-responsive neurons in areas 17 and 18 of cat. J. Neurophysiol. *72*, 2134–2150.
Zipser, K., Lamme, V.A.F., Schiller, P.H., 1996. Contextual modulation in primary visual cortex. J. Neurosci. *16*, 7376–7389.